Supporting Information

A comprehensive UHPLC ion mobility QTOF method for profiling and quantification of eicosanoids, other oxylipins and fatty acids.

Christine Hinz,[†,○] Sonia Liggi,[†,○] Gabriele Mocciaro,[†] Stephanie Jung,[‡] Isuru Induruwa,[§] Milton Pereira,[‖] Clare E. Bryant,[‖] Sven W. Meckelmann,[⊥] Valerie B. O'Donnell,[#] Richard W. Farndale,[‡] John Fjeldsted,[∇] Julian L. Griffin[*,†]

○ C.H. and S.L. contributed equally to this work

† Department of Biochemistry and Cambridge Systems Biology Centre, University of Cambridge, Cambridge CB2 1GA, United Kingdom

‡ Department of Biochemistry, University of Cambridge, Downing Site, Cambridge CB2 1QW, United Kingdom

§ Department of Clinical Neurosciences, University of Cambridge, CB2 0QQ, United Kingdom

‖ Department of Veterinary Medicine, University of Cambridge, Cambridge CB3 0ES, United Kingdom

⊥ University of Duisburg-Essen, Faculty of Chemistry, Applied Analytical Chemistry, 45141 Essen, Germany

Cardiff University, Systems Immunity Research Institute, Cardiff CF14 4XN, United Kingdom

∇ Agilent Technologies, Santa Clara, CA 95051, United States

* To whom correspondence should be addressed; e-mail: jlg40@cam.ac.uk.

Table of Contents

SUPPORTING MATERIALS S-3
Isolation and thrombin stimulation of human platelets S-3
BMDM isolation and culture S-3
BMDM infection S-3
SUPPORTING DISCUSSION S-4
Non-specific water losses during LCMS analysis of lipids S-4
Comparison between annotation in DTIM and LCMS S-4
Table S2 ..... S-6
Table S3 ..... S-6
Table S8 ..... S-7
Figure S1 ..... S-8
Figure S2 ..... S-9
Figure S3 ..... S-10
Figure S4 ..... S-11
Figure S5 ..... S-12
Figure S6 ..... S-13
Figure S7 ..... S-14
Figure S8 ..... S-15
Figure S9 ..... S-16
Figure S10 ..... S-17
Figure S11 ..... S-18
Figure S12 ..... S-19
Figure S13 ..... S-20
References S-21

SUPPORTING MATERIALS

Isolation and thrombin stimulation of human platelets. Three healthy volunteers were selected for this study if they were not taking anti-inflammatory medications in the week before sample collection. Thirty mL of blood was drawn from the antecubital vein of the volunteers, mixed with acid-citrate-dextrose (ACD) buffer (85 mM trisodium citrate, 65 mM citric acid, 100 mM glucose) at a ration 8.1:1.9 (v/v, blood:ACD) and centrifuged at 250 *g* for 15 min at room temperature. The platelet rich plasma was collected and centrifuged at 900 *g* for 12 min at room temperature. After the supernatant was discarded, the platelets were resuspended with calcium-free Tyrode's buffer (134 mM/L NaCl, 12 mM/L $NaHCO_3$, 2.9 mM/L KCl, 0.34 mM/L Na_2HPO_4, 1.0 mM/L $MgCl_2$,10 mM/L HEPES, 5 mM/L glucose; pH 7.4) containing 10 % ACD and centrifuged at 900 *g* at room temperature for 12 min. The pellet was resuspended in 2 mL Tyrode's buffer and platelet count adjusted to $2x10e^{08}$ platelets/mL. Platelets were incubated with 1 mM $CaCl_2$ for 5 min at 37°C before treatment with 0.2 U/mL thrombin for 1h at 37°C. Some samples were pre-incubated with 100 mM aspirin or equal volumes ethanol as vehicle control.

BMDM isolation and culture. Mice were killed by cervical dislocation, sprayed with ethanol 70% for sterilization and their hind legs without the skin were aseptically removed and placed in Dulbecco's modified Eagle's medium (DMEM) on ice. In a laminar flow cabinet, muscle and connective tissue surrounding the bones were removed, the tibia and femur were separated at the knee joint with the proximal and distal epiphysis removed. Bone marrow was flushed out with the help of a 25G syringe using BMDM growth media (DMEM supplemented with 10% fetal bovine serum, 20% L929 conditioned media and 5 mM L-Glutamine). The collected cells were centrifuged at 300 *g* for 10 min at 15°C and resuspended in BMDM growth media. After 6 days in culture, the petri dishes containing BMDMs were washed three times in plain media, the cells were then carefully scrapped and resuspended in BMDM growth media. Next, $5x10^6$ cells were plated on 6-well plates and incubated overnight at 37°C under 5% CO_2.

L929 conditioned media was prepared by growing L929 cells to confluence for 2 weeks, in RPMI 1640 medium supplemented with 10% fetal bovine serum and 5 mM L-glutamine. The culture supernatant was collected and sterilized by filtration through 0.22 μm filters with a polyethersulfone membrane (Millipore, Merck KGaA, Darmstadt, Germany).

BMDM infection. Prior to infection, BMDMs were primed with 200 ng/mL ultrapure LPS from *Escherichia coli* O111:B4 (InvivoGen) for 3 hours at 37°C and 5% CO_2, followed by three washes in LPS-free media. *Salmonella enterica* serovar Typhimurium strain SL1344 was cultured to log phase by pre-culturing the bacteria for 17.5 hours in 5 mL lysogeny broth (LB) at 37°C and 200 rpm, followed by a 1 in 10 dilution of the pre-culture in LB broth and further culture for 2 hours. The bacteria were then centrifuged for 10 min at 4,300 *g* and resuspended in BMDM growth media. Next, the bacteria solutions were diluted to multiplicity of infection (MOI) 10 in BMDM growth media and used for infections for 1 hour. MOI was confirmed by plating the bacteria in LB agar for 16 hours at 37°C. After infection, the supernatant was collected and cellular debris was removed by centrifugation for 10 min at 12,000 g and 4°C.

SUPPORTING DISCUSSION

Non-specific water losses during LCMS analysis of lipids. The case of non-specific losses such as water is a complex matter and requires careful consideration. In this study, we observed $[M\text{-}H\text{-}H_2O]^-$ and $[M\text{-}H\text{-}2H_2O]^-$ for some lipids in full scan data, whose appearance was not due to too harsh ionization conditions as different ion source parameters did not affect their abundancy (data not shown). Moreover, in source fragmentation would theoretically result in $[M\text{-}H]^-$, $[M\text{-}H\text{-}H_2O]^-$ and $[M\text{-}H\text{-}2H_2O]^-$ species separating in DT due to their different *m/z*. However, flow injection DTIMS acquisition of PGE_2 standard results in coelution and codrift, and hence similar CCS values between the water loss species and the $[M\text{-}H]^-$ ions (see Figure 1 in section "Ion Mobility Allows Identification of Lipid Clusters" of the manuscript). These observations lead to our hypothesis that fragmentation, and therefore change in *m/z*, occurs after DT separation.

Apart from the flow injection data of lipid standards presented in the manuscript, we also observed this phenomenon in LC-DTIM-MS acquisition of biological samples. For instance, in the BMDM data (table S4), met_271 is identified as the most abundant $[M\text{-}H]^-$ species for PGE_2, with RT = 4.486 min and CCS = 185.47 $Å^2$. This species not only coelutes and codrifts with met_297 and met_273, whose *m/z* correspond to $[M\text{-}H\text{-}H_2O]^-$ and $[M\text{-}H\text{-}2H_2O]^-$ species of PGE_2, respectively, but also shares very similar CCS values with them (ΔCCS = 1.13 for met_297 and 0.06 for met_273). The coelution and minor differences in CCS values between $[M\text{-}H]^-$ and the aforementioned species, as well as the lack of variation in signal intensity when changing source parameters, supports our initial hypothesis about these signals deriving from post-drift tube loss of water rather than from different molecules.

Loss of water is only observed for a sub-set of the lipids analyzed, therefore it may be a species-specific pattern related to different structural rearrangements, as recently discussed.[1] However, these different conformations could also result in similar drift behaviour for species with different *m/z*. Indeed, the mobility behavior of ions depends not only on their *m/z* but also on their shape. For instance, most of the species observed for PGE_2 have very similar DT and CCS values to those detected for PGJ_2, which is 18 Da lighter. More specifically, in the BMDM data met_271 (PGE_2 $[M\text{-}H]^-$) differs from met_2365 (most abundant signal for PGJ_2 $[M\text{-}H]^-$) in RT and *m/z*, but the two species share a similar CCS value (ΔCCS = 0.25). In contrast, met_297 (PGE_2 $[M\text{-}H\text{-}H_2O]^-$) has the same *m/z* and similar CCS value to met_2365 but was correctly not assigned as such due to different RTs (4.485 min for the former *versus* 7.081 min for the latter). In the first step of feature identification from the internal library met_297 was annotated as PGJ_2 $[M\text{-}H]^-$ and successively corrected to PG-like given RT mismatch. Indeed, the RT threshold in feature identification (±0.15 min) was set based on the concept that coeluting species must have similar physico-chemical properties, hence the different elution behavior of met_273 and met_2365 further support our hypothesis that met_273 is a loss of water product of PGE_2 rather than $[M\text{-}H]^-$ species of PGJ_2. Furthermore, these findings show that loss of water, hence a lighter ion, does not necessarily yield a smaller CCS value due to possible molecular rearrangements, and at the same time these results highlight the importance of LC separation for these lipids, as DTIM-MS alone could lead to misassignment of some molecular features.

Although identification and complete understanding of the mechanisms driving the formation of these species may not be trivial, the addition of DT dimension and hence CCS can help gain further insights into non-specific losses as well as increase their annotation confidence compared to LC/MS/MS alone, which in common targeted approaches requires identification of precursor ions prior the analysis and consequently longer development time. All the information here presented has a potential for the automated identification of water loss species. However, as not all lipids analyzed present these species, we did not insert them in the database for the time being. To further improve identification of non-specific water losses as well as oxylipins in general, future work will involve inclusion of MS/MS data as well as expansion of the lipid standards library. Moreover, combination of these experimental observations with *in-silico* studies such as CCS evaluations and molecular dynamics simulations could be useful to further unravel these phenomena and potentially provide increased confidence in non-specific loss identification.

Comparison between annotation in DTIM and LCMS. Processing of biological samples acquired with DTIM with the MassHunter Mass Profiler software yields a large number of features, out of which only a relatively small percentage can be identified or annotated with actual molecules. For instance, in the *S.* Typhimurium-infected murine bone-marrow-derived macrophages (BMDMs) dataset, 3339 features were found by the peak picking algorithm. Eighty-five of these could be identified by our protocol (i.e. their *m/z*, RT and CCS values matched those in the internal database obtained from lipid standards), 146 were flagged as lipid-like (i.e. their *m/z* as well as either their CCS or their RT matched those in the internal database), 624 could be annotated with LIPID MAPS (i.e. only *m/z* could be matched with the external database, which is not enough to identify a molecule given the presence of isomeric species), and finally 2484 species remained unknown (and may not be lipids). Given these high numbers of detected features and unknowns, we decided to compare these results with those that would have been obtained in a standard LC-MS analysis. Please note that we can only compare annotation (i.e. match between *m/z* detected in our samples and *m/z* of compounds present in an external library) and not identification (*m/z*, RT and DT match with internal library) given the lack of mobility dimension in LC-MS. We did this by processing the BMDMs dataset with the MassHunter Profinder software, which ignores the mobility dimension, followed by the same post processing pipeline used for DTIM data. In this case, the number of detected "features" is 580, with 177 of them annotated with LIPID MAPS. Please note the use of the quotes around the term features: Profinder groups coeluting and related features, outputting compound groups (containing all the related and coeluting adducts, isotopes, etc.) as opposed to all the features detected in the dataset. Hence, the nearly 6-fold reduction in features outputted by Profinder compared to Mass Profiler is not only due to the omission

of the mobility dimension by the algorithm of the former, but also by the different characteristics of the two algorithms. Nonetheless, comparison with the DTIM data can still be performed on the number of unique LIPID MAPS identifiers. Many of the 177 compound groups annotated with LIPID MAPS present multiple annotations, resulting in a total of 818 unique LIPID MAPS identifiers. Similarly, out of the 3339 features detected with DTIM, 864 were annotated or identified with at least one compound, resulting in 1455 unique LIPID MAPS identifiers. Of these, 790 are in common between DTIM and LC-MS (26 of which are present in the internal library), 664 are found only in DTIM and 28 only in LC-MS (Figure S12). Among the 28 identifiers found only in LC-MS, 8 lipids present in our internal library (namely 12-HEPE, 6-keto-PGF1-alpha, 13-HODE, 13-HpODE, 12(13)-EpOME, 9(10)-EpOME, 11(12)-EET and 8(9)-EET) are annotated with 17 features. However, the difference in RT between these 17 features and the lipids in our internal library exceeds the ± 0.15 min threshold set for identification, hence why they are not found in the DTIM data and we can confidently consider them as wrongly annotated. On the other hand, the remaining 20 lipids annotated only in the LC-MS data as well as the 664 LIPID MAPS identifiers found only in DTIM are instead annotated with respectively 3 and 232 features which could not be found with similar m/z and RT in the other dataset, probably due to the different algorithms used by the 2 feature finding programs. Overall, out of the total 1483 LIPID MAPS identifiers annotated with either DTIM or LC-MS data, 53.35% were found to be overlapping, 1.9% were found only in LC-MS (including also the 8 wrongly annotated compounds), and 44.75% only in the DTIM data.

Table S1, 4, 5, 6 and 7 are provided as xlsx documents

Table S1: Oxylipin and fatty acids library. Lipid standards were analyzed using LC-DTIM-MS to generate a database containing $^{DT}CCS_{N2}$ and retention time values for the several conformers of the 47 lipid standards, along with other molecular structural (2D) and commercial information, to be used for annotation with the KniMet "Feature Annotation from internal IMS DB" functionality.

Table S2: Upper and lower limits of quantification (ULOQ and LLOQ, respectively) on column, regression coefficient (R^2) and internal standard (IS) used for a range of oxylipins and fatty acids. The limit of quantification was defined as signal-to-noise ≥ 9. ULOQ: highest amount of standard analyzed.

Lipid	LLOQ [ng]	LLOQ [nM]	ULOQ [ng]	ULOQ [nM]	R^2	IS
PGE_2	0.020	11.349	5.000	2837.160	0.998	PGE2-d4
6-keto-PGF1α	0.020	11.220	5.000	2805.049	0.990	6-keto PGF1α-d4
12-HETE	0.010	6.241	5.000	3120.417	0.997	12-HETE d8
15-HETE	0.010	6.241	5.000	3120.417	0.997	15-HETE d8
5(6)-EET	0.001	0.624	5.000	3120.417	0.999	5-HETE d8
8(9)-EET	0.001	0.624	5.000	3120.417	0.996	5-HETE d8
11(12)-EET	0.001	0.624	5.000	3120.417	0.998	5-HETE d8
9(10)-EpOME	0.001	0.675	5.000	3372.681	0.998	5-HETE d8
11,12-DHET	0.002	1.182	5.000	2954.210	0.997	15-HETE d8
Linoleic Acid	0.001	0.713	5.000	3565.755	0.992	arachidonic acid d8
α-Linolenic Acid	0.001	0.718	5.000	3591.567	0.998	arachidonic acid d8
Stearidonic Acid	0.001	0.724	5.000	3617.945	0.997	arachidonic acid d8
Dihomo-ɣ-Linolenic Acid	0.001	0.653	5.000	3262.749	0.995	arachidonic acid d8
Arachidonic acid	0.001	0.657	5.000	3284.429	0.983	arachidonic acid d8
Eicosapentaenoic Acid	0.001	0.661	5.000	3306.321	0.997	arachidonic acid d8
Docosahexaenoic acid	0.001	0.609	5.000	3044.251	0.995	arachidonic acid d8

Table S3: Absolute concentrations (ng/5x10^5 cells) of oxylipins and fatty acids in *S.* Typhimurium-infected murine bone-marrow-derived macrophages (BMDMs). Values represent mean (n=3) ± SEM. Some lipids were not detected (n.d.) under certain conditions.

	ng/5x10^5 cells			SEM		
	BMDM, untreated	*S.* Typhimurium only	BMDM, *S.* Typhimurium	BMDM, untreated	*S.* Typhimurium only	BMDM, *S.* Typhimurium
PGE_2	1.328	n.d.	18.825	0.554	-	4.439
5(6)-EET	0.092	0.040	1.046	0.127	0.124	0.480
Docosahexaenoic acid	3.794	0.257	27.582	2.456	0.000	2.464
alpha-Linolenic Acid	0.332	0.042	0.236	0.362	0.082	0.375
Eicosapentaenoic Acid	0.719	0.013	4.936	0.156	0.000	0.325
Dihomo-ɣ-Linoleic Acid	0.014	n.d.	0.172	0.016	-	0.050
Arachidonic Acid	0.045	0.045	31.109	0.000	0.000	3.806

Table S4: Features found in *S.* Typhimurium-infected BMDMs. Lipid extracts of BMDMs were analyzed using LC/IM-MS and processed using the MassHunter Suite and KniMet (missing value imputation performed with the KNN method). Features (mass-to-charge ration, retention time, drift time, and $^{DT}CCS_{N2}$) were annotated using an internal database as well as LIPID MAPS.

Table S5: Features driving PCA separation between the three classes of samples (Uninfected, Infected and Infected Media) for the *S.* Typhimurium-infected BMDMs study.

Table S6: Features driving PCA separation between the four classes of samples (Untreated, Ethanol, Aspirin and Thrombin) for the human isolated platelets study.

Table S7: Features found in human platelets. Lipid extracts of human platelets subjected to four different treatments were analyzed using LC/IM-MS and processed using the MassHunter Suite and KniMet (missing value imputation performed with the KNN method). Features (mass-to-charge ration, retention time, drift time, and $^{DT}CCS_{N2}$) were annotated using an Internal database as well as LIPID MAPS.

Table S8: The $^{DT}CCS_{N2}$ obtained for the $[M-H]^-$ species of the standards acquired internally were compared with the values recently published.[1–3] The table reports for each lipid the published $^{DT}CCS_{N2}$ value, the source of the value, the internally obtained value, the Relative Standard Deviation (RSD) between the internal and external value, along with common name, monoisotopic molecular mass and LIPID MAPS identifier of the molecule.

External CCS (Å²)	Source	Internal CCS (Å²)	RSD (%)	Name	Monoisotopic molecular mass (Da)	LIPID MAPS ID
185	Kyle et al.	179.75	2.04	11(12)-EET	320.24	LM:LMFA03090010
182	Di Giovanni et al.	181.06	0.37	11-HETE	320.24	LM:LMFA03060003
184.1	Kyle et al.	178.86	2.04	12-HETE	320.24	LM:LMFA03060007
184	Di Giovanni et al.	178.86	2.00	12-HETE	320.24	LM:LMFA03060007
182.13	Kyle et al.	190.08	3.02	13-HODE	296.24	LM:LMFA02000035
182	Di Giovanni et al.	183.12	0.43	15-HETE	320.24	LM:LMFA03060001
186.2	Kyle et al.	182.26	1.51	5-HETE	320.24	LM:LMFA03060002
185	Di Giovanni et al.	182.26	1.06	5-HETE	320.24	LM:LMFA03060002
196.7	Kyle et al.	191.12	2.03	6-keto-PGF1alpha	370.24	LM:LMFA03010001
184.63	Kyle et al.	179.39	2.04	8(9)-EET	320.24	LM:LMFA03080003
185.07	Kyle et al.	180.67	1.70	8-HETE	320.24	LM:LMFA03060006
182	Di Giovanni et al.	180.67	0.52	8-HETE	320.24	LM:LMFA03060006
197.25	Kyle et al.	191.54	2.08	8-iso-PGF2-alpha	354.24	LM: LMFA03110001
182.21	Kyle et al.	179.14	1.20	Arachidonic Acid	304.24	LM:LMFA01030001
187.44	Kyle et al.	182.81	1.77	LTB4	336.23	LM:LMFA03020001
183	Di Giovanni et al.	182.81	0.07	LTB4	336.23	LM:LMFA03020001
226.23	Kyle et al.	221.02	1.65	LTD4	496.26	LM:LMFA03020006
190.07	Kyle et al.	183.89	2.38	PGD2	352.22	LM:LMFA03010004
192.06	Kyle et al.	193.04	0.36	PGE2	352.22	LM:LMFA03010003
194.77	Kyle et al.	187.65	2.63	PGF2-alpha	354.24	LM:LMFA03010002
183.66	Stow et al.	179.14	1.76	Arachidonic Acid	304.24	LM:LMFA01030001
183.02	Stow et al.	178.83	1.64	Dihomo-gamma-Linolenic Acid	306.26	LM:LMFA01030158
154.82	Stow et al.	167.57	5.59	Lauric Acid	200.18	LM:LMFA01010012
175.69	Stow et al.	171.78	1.59	Linoleic Acid	280.24	LM:LMFA01030120
176.46	Stow et al.	172.52	1.60	Oleic Acid	282.26	LM:LMFA01030002
169.12	Stow et al.	166.02	1.31	Palmitic Acid	256.24	LM:LMFA01010001
167.95	Stow et al.	164.9	1.30	Palmitoleic Acid	254.22	LM:LMFA01030055
177.66	Stow et al.	174.29	1.35	Stearic Acid	284.27	LM:LMFA01010018
174.88	Stow et al.	178.57	1.48	alpha-linolenic acid	278.22	LM:LMFA01030152

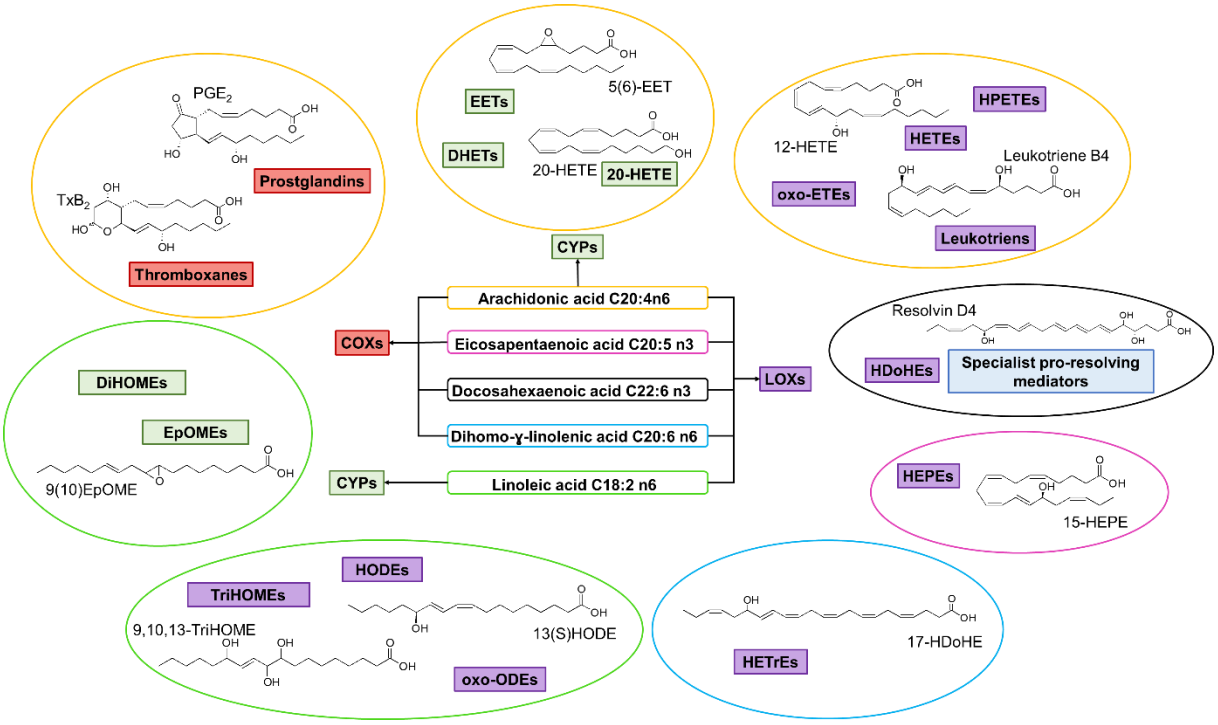

Figure S1: Oxylipin network and their fatty acid precursors. Unsaturated fatty acids arachidonic acid (yellow), eicosapentaenoic acid (pink), docosahexaenoic acid (black), dihomo-ɣ-linolenic acid (blue), and linoleic acid (light green), can be oxidized to a variety of oxylipins by cytochrome P450 (CYPs, dark green), cyclooxygenases (COXs, red), lipoxygenases (LOXs, purple). Examples of oxylipins deriving from each fatty acid and enzyme group are marked in the color of the enzymes responsible for their generation, for instance prostaglandins are marked red as they are generated by COXs. Circles around oxylipin groups are colored in the color code of the fatty acid they derive from. Specialist pro-resolving mediators (blue) are generated by a combination of enzymes.

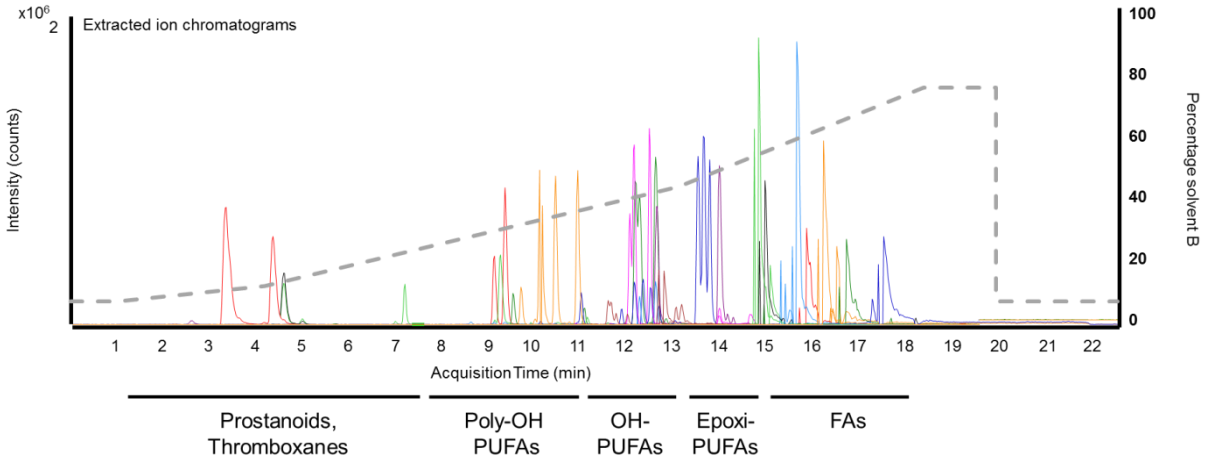

Figure S2: Extracted ion chromatograms of oxylipin and fatty acid standards. Lipids were analyzed using a 22 min RP gradient separation (grey, dashed) and their accurate mass extracted (± 10 ppm). Oxylipins and fatty acids elute according to their polarity, with prostaglandins and thromboxanes eluting first, followed by poly-hydroxy (OH)-polyunsaturated fatty acids (PUFAs), hydroxyl-PUFAs, Epoxi-PUFAs and fatty acids (FA).

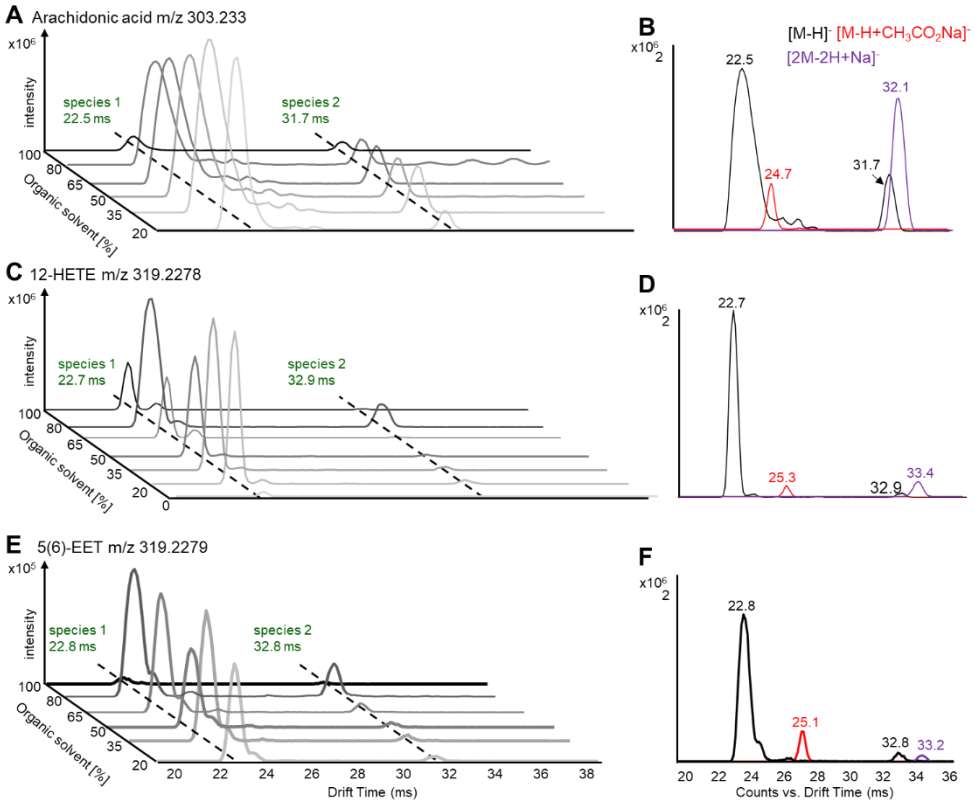

Figure S3: DTIMS separates both oxylipin and fatty acid aggregates. Standards of arachidonic acid, 12-HETE, and 5(6)-EET were analyzed by DTIM-MS following flow injection using an organic solvent mixture (acetonitrile: methanol, 6:1, v/v) in varying concentrations. For each lipid standard, the intensity of the two species whose *m/z* correspond to the $[M\text{-}H]^-$ conformer is plotted versus the DT and the concentration of organic solvent (A, C, E), with their average drift times shown in green. The drift spectra for the conformers $[M\text{-}H]^-$ (black), $[M\text{-}H+CH_3CO_2Na]^-$ (red), and $[2M\text{-}2H+Na]^-$ (purple) observed for observed for arachidonic acid (B), 12-HETE (D), and 5(6)-EET (F).

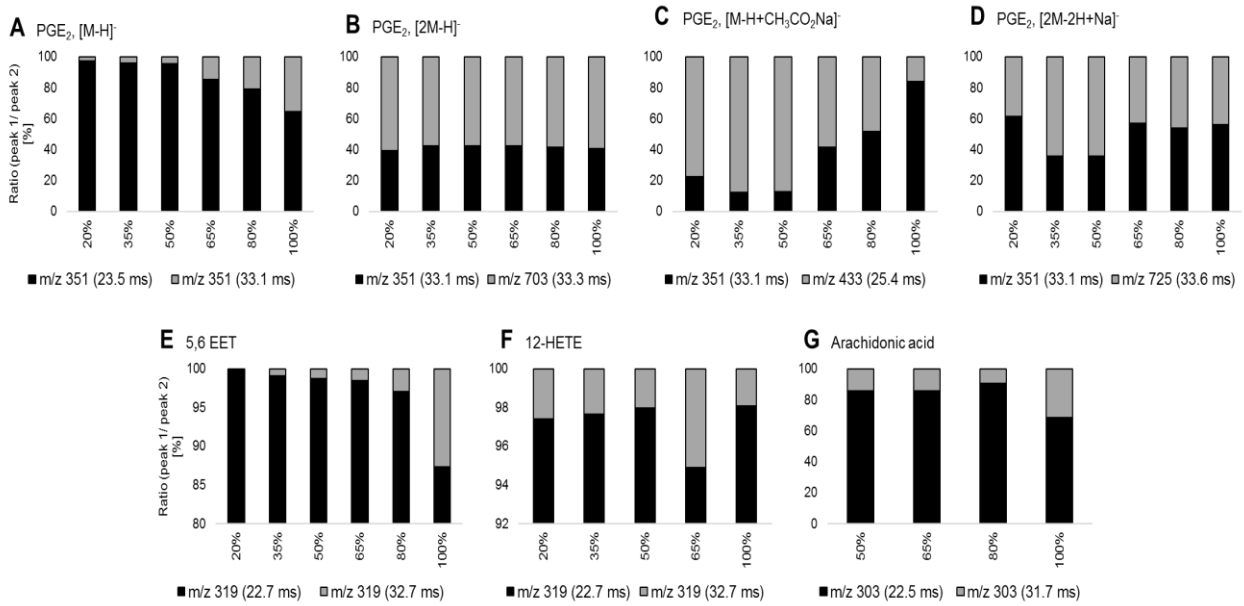

Figure S4: The formation of both second [M-H]$^-$ species and sodium acetate adducts in drift spectra depends on the organic solvent content. Several oxylipins standards were analyzed by flow injection DTIM-MS at different concentrations of organic solvent (20, 35, 50, 65, 80 and 100%) to evaluate the intensity variation of their conformers. In particular, the ratio of drift peak area between the first and second [M-H]$^-$ species of PGE_2 (*m/z* 351.2167, DT 23.5 ms and 33.1 ms, respectively), as well as the ratio between the drift peak area of the second [M-H]$^-$ species and [2M-H]$^-$ (*m/z* 703.4422), [M-H+CH_3CO_2Na]$^-$ (*m/z* 433.2205), and [2M-2H+Na]$^-$ (*m/z* 725.4250) are plotted (A-D). Similarly, the drift peak areas of the first and second [M-H]$^-$ species for EET (*m/z* 319.2279), 12-HETE (*m/z* 319.2271), and arachidonic acid (*m/z* 303.2319) are showed in (E-G). These plots show how the intensity of both second [M-H]$^-$ species and sodium acetate adducts increases with an increase in the organic solvent content, while this is not observed for dimers

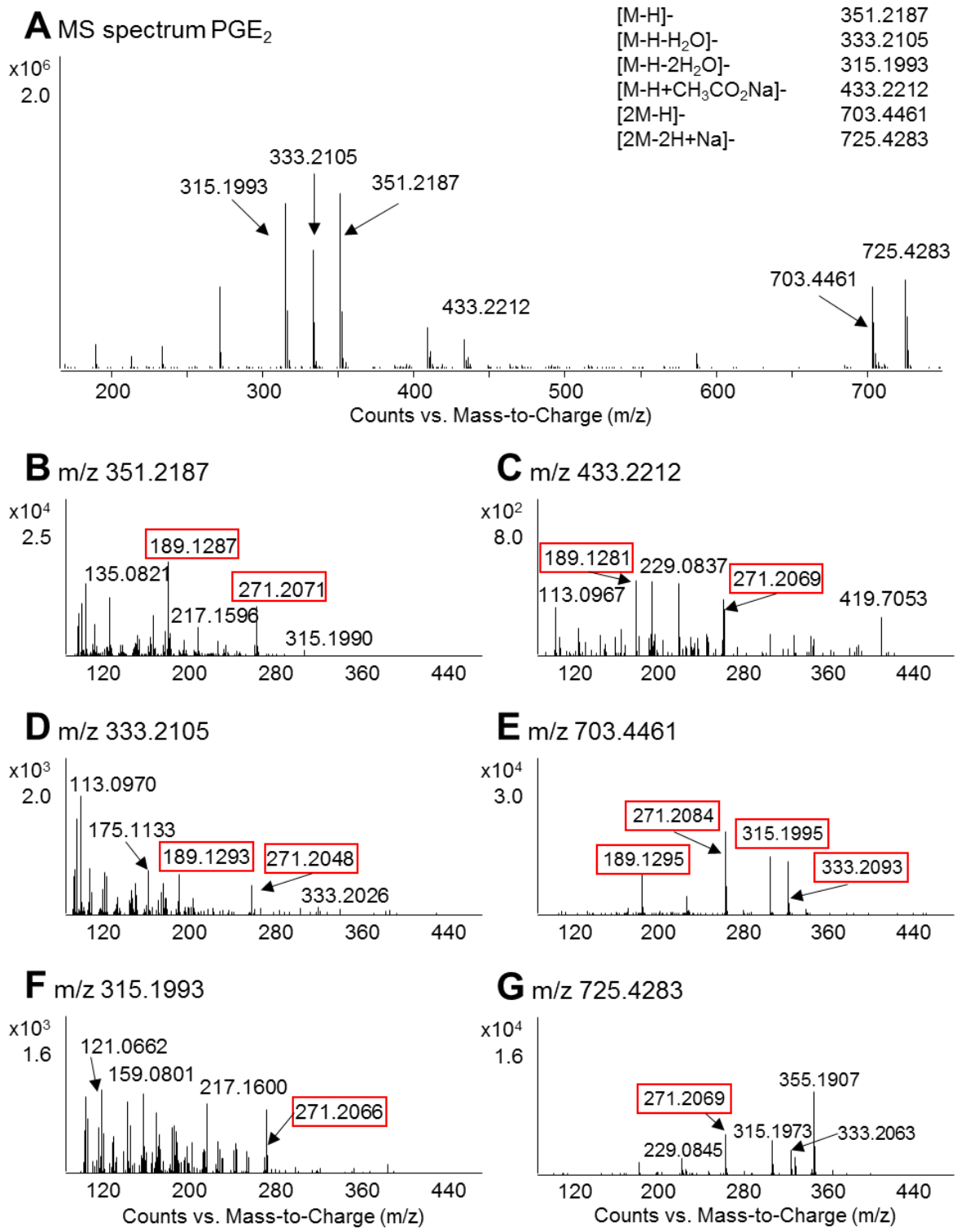

Figure S5: Fragmentation of PGE_2 adducts and aggregates leads to diagnostic product ions. PGE_2 standard was analyzed by flow injection DTIM-MS/MS. All the product ion spectra of the species observable in the MS spectrum of PGE_2 (A), namely (B) $[M-H]^-$, (C) $[M-H+CH_3CO_2Na]^-$, (D) $[M-H_2O]^-$, (E) $[2M-H]^-$, (F) $[M-2H_2O]^-$, and (G) $[2M-2H+Na]^-$, present the diagnostic fragment ions *m/z* 189.129 and *m/z* 271.207 (marked in red).

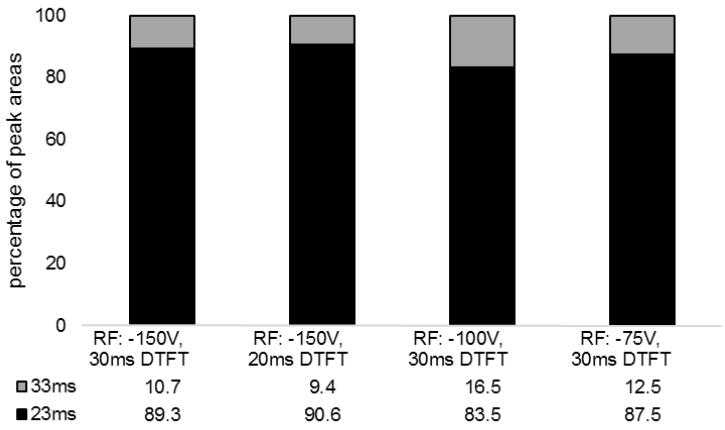

Figure S6: The formation of the second [M-H]$^-$ species in drift spectra does not depend on drift tube fill time and trap funnel RF alone. PGE_2 standard was analyzed by flow injection DTIM-MS with different drift tube fill time (DTFT, 30 and 20 ms) and trap funnel RF voltages (-150, -100 and -75 V) to evaluate if the intensity of the two [M-H]$^-$ conformers observed in drift spectra of oxylipins was affected by the variation of these parameters. The bar plot shows that formation of the two species is not affected by reduction of neither the drift tube fill time nor the trap funnel RF voltage.

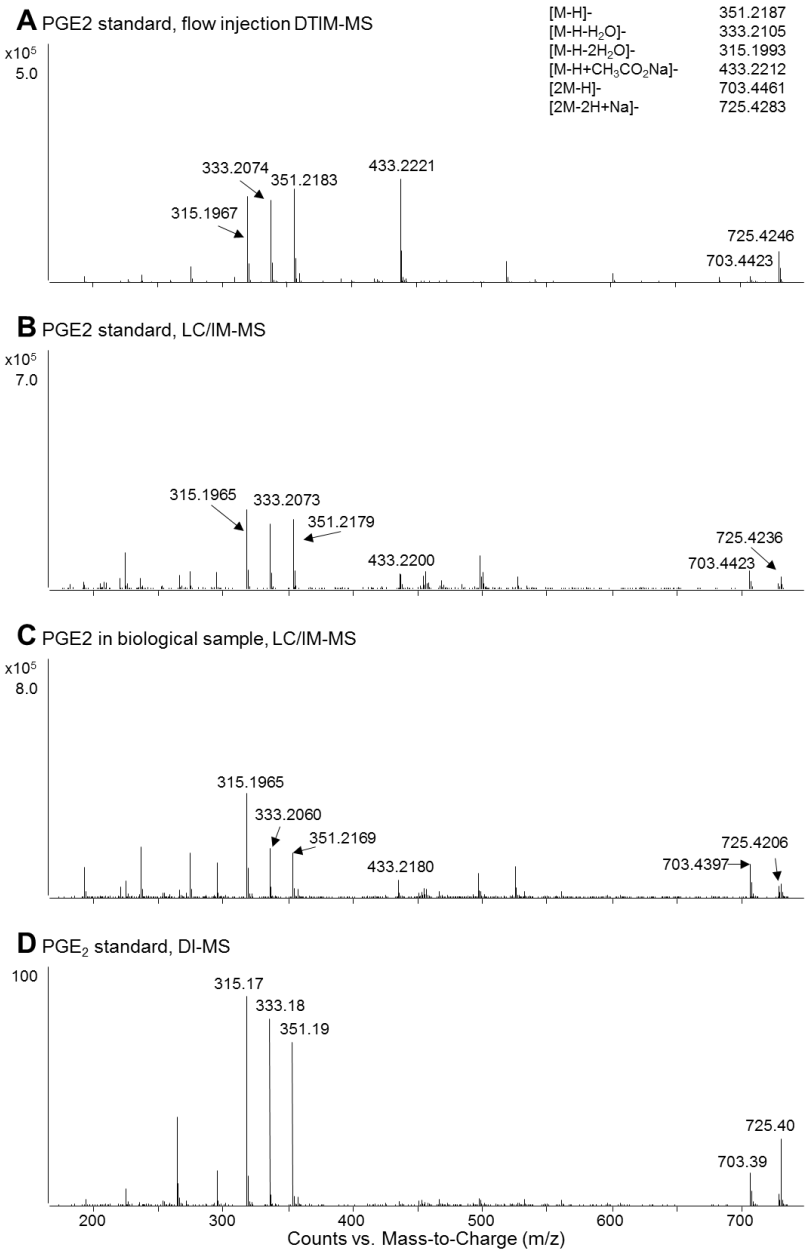

Figure S7: PGE_2 aggregates are observed in both lipid standards and biological samples. PGE_2 standard has been analyzed by (A) flow injection DTIM-MS and (B) LC/IM-MS, showing in both cases the presence of *m/z* 351.2177 $[M\text{-}H]^-$, *m/z* 433.2206 $[M\text{-}H+CH_3CO_2Na]^-$, *m/z* 703.4427 $[2M\text{-}2H+Na]^-$, and *m/z* 725.4247 $[2M\text{-}2H+Na]^-$, as well as the water-loss species *m/z* 315.1967 $[M\text{-}H\text{-}2H_2O]^-$ and *m/z* 333.2074 $[M\text{-}H\text{-}H_2O]^-$. Moreover, the same species can be observed also in the spectrum of PGE_2 in lipid extract of (C) a biological sample and in (D) the spectrum obtained from PGE_2 standard analyzed using direct infusion (DI) in full scan negative ion mode on a Thermo Scientific TSQ Quantiva platform.

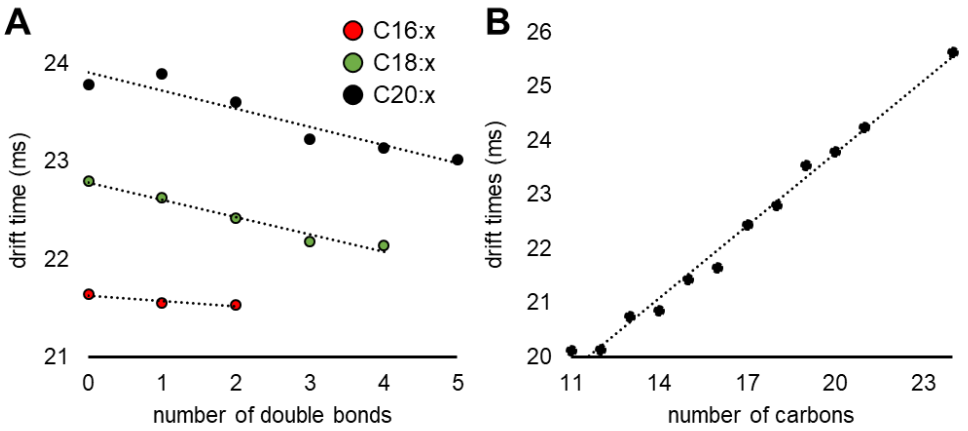

Figure S8: The drift behavior of fatty acids depends on their chain length and degree of unsturation. (A) Unsaturated fatty acid containing 16, 18 and 20 carbon atoms analyzed by DTIM-MS showed a linear correlation between the number of double bonds in their chain and their DT. A linear correlation is observed also between DTs of saturated fatty acids and their chain length (B).

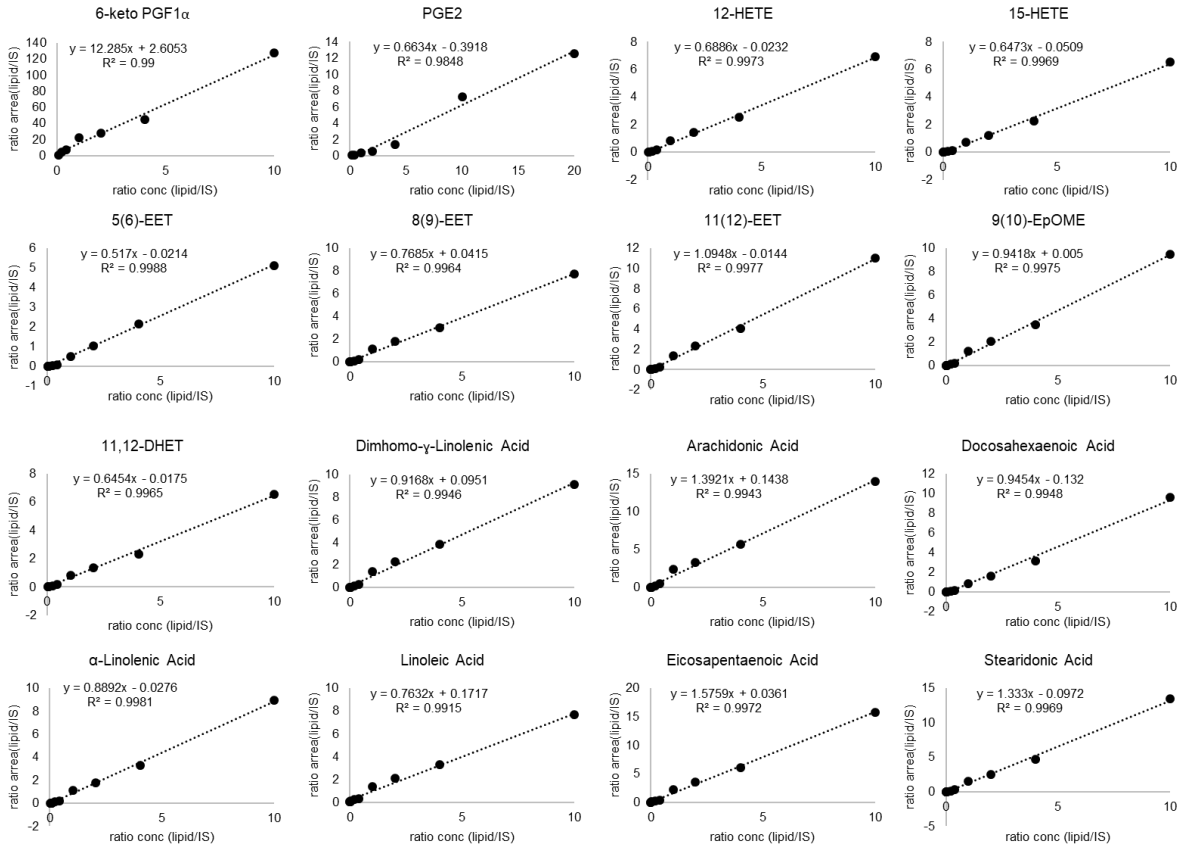

Figure S9: Calibration curves of oxylipins and fatty acids included in the quantitation method. Lipid standards were analyzed within their LOQ ranges (Table S2) and calibration curve calculated using a linear curve fit, not forced through zero. All coefficients of regression are $R^2 > 0.99$ (except for PGE2, with $R^2 = 0.9848$).

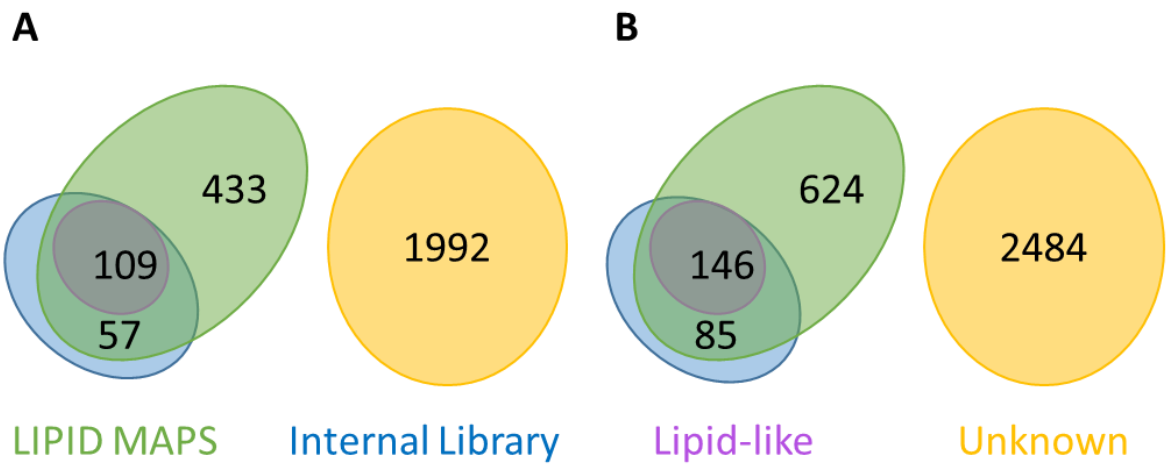

Figure S10: Overlap between internal database and LIPID MAPS. The Venn diagrams show the overlap between the features annotated with the fatty acids portion of the LIPID MAPS Structure database (green circles) and those identified by comparison with the Internal database (blue circles), along with the lipid-like flags (purple circles) and the unknowns (yellow circles) for (A) BMDBs and (B) platelets case studies.

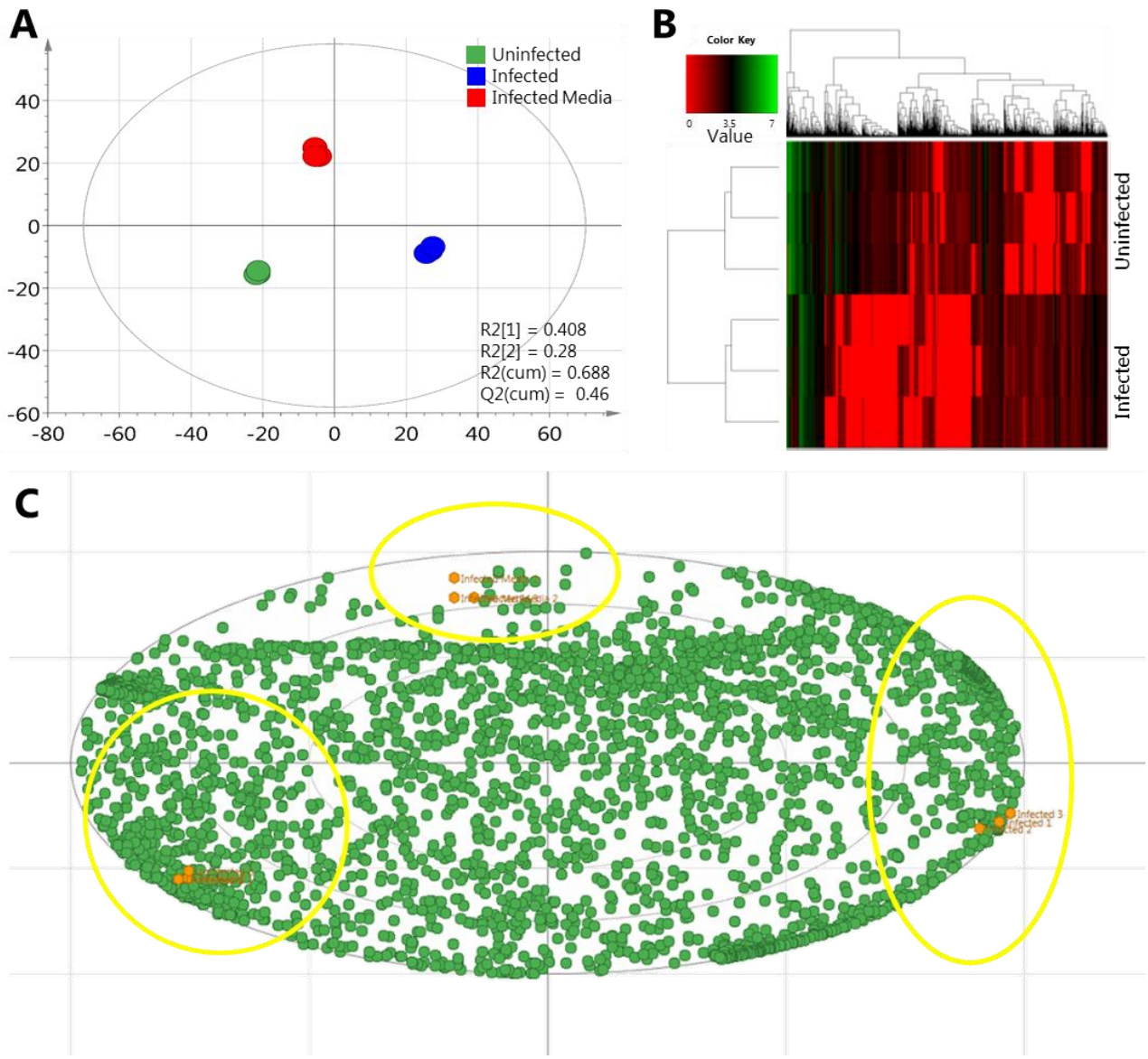

Figure S11: BMDM samples separate according to infection. (A) Score plot of the principal component analysis (first *versus* second PC) of lipid extracts of BMDM cells either infected with *S.* Typhimurium (blue), not infected (green), as well as infected culture medium (red), analyzed by LC-DTIM-MS. (B) Heatmap representation and hierarchical clustering of the distance matrix between Infected and Uninfected samples. In both plots it is possible to observe a clear separation between Infected and Uninfected samples, which form distinct clusters in the heatmap and are separated according to the first component in PCA. (C) Biplot showing overlap between the score plot and the loading plot obtained from PCA of the BMDMs *S.* Typhimurium-infected samples. Yellow circles highlight the compounds driving separation between samples, which are also listed in Table S5.

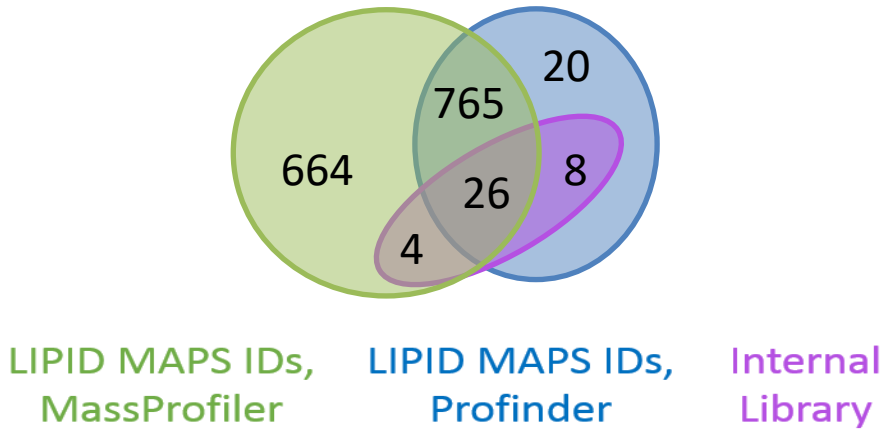

Figure S12: Overlap between annotation in LC-IM-MS and LC-M data. The BMDMs dataset was processed with two different software packages from the MassHunter suite: Mass Profiler, which takes into consideration the mobility dimension, and Profinder, which only considers LC-MS. The Venn diagram shows the overlap between the unique LIPID MAPS identifiers annotated with the DTIM data (green circle) and those annotated with the LC-MS data (blue circle). Among these identifiers, 38 correspond to lipids present in the internal library (purple circle). The portion of LIPID MAPS identifiers not overlapping between the two processing methods derives from the different characteristics of the algorithms used.

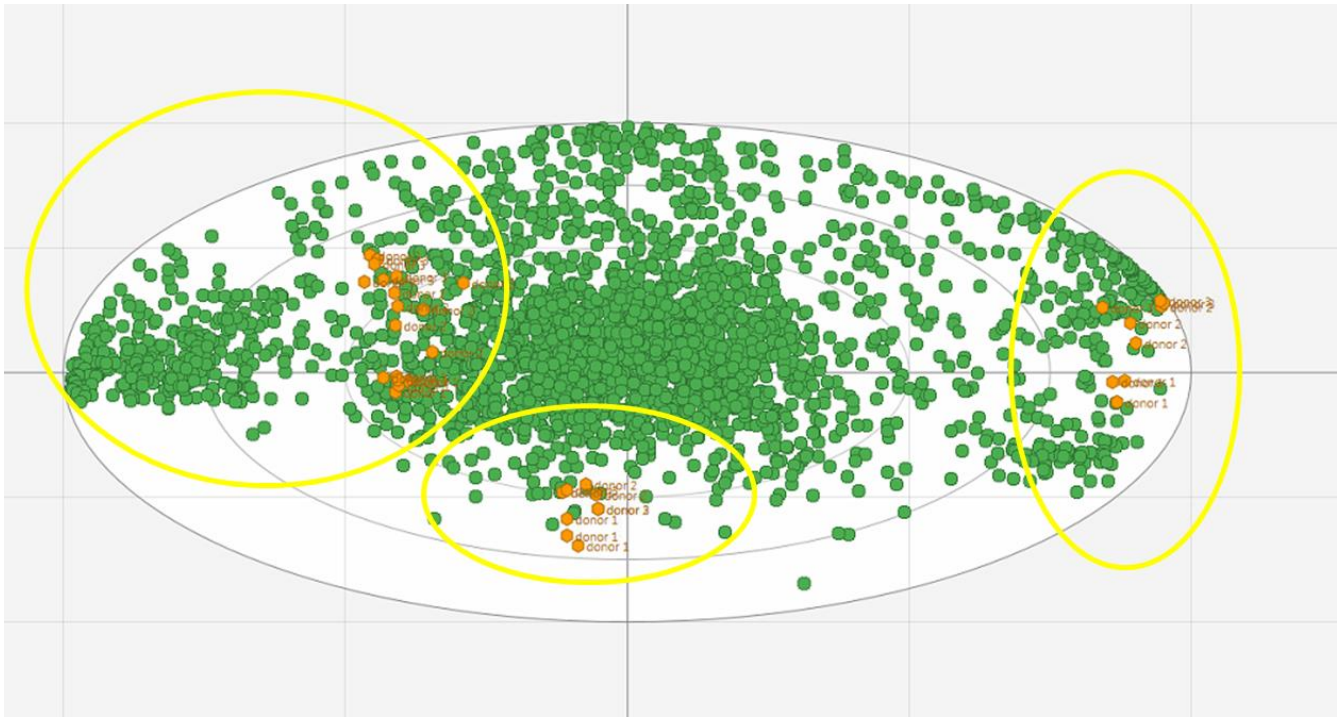

Figure S13: Biplot showing overlap between the score plot and the loading plot obtained from PCA of the human isolated platelet samples. Yellow circles highlight the compounds driving separation between samples, which are also listed in Supporting Table 6.

REFERENCES

(1) Di Giovanni, J. P.; Barkley, R. M.; Jones, D. N. M.; Hankin, J. A.; Murphy, R. C. Tandem Mass Spectrometry and Ion Mobility Reveals Structural Insight into Eicosanoid Product Ion Formation. *J. Am. Soc. Mass Spectrom.* **2018**, *29* (6), 1231–1241. https://doi.org/10.1007/s13361-018-1927-9.

(2) Kyle, J. E.; Aly, N.; Zheng, X.; Burnum-Johnson, K. E.; Smith, R. D.; Baker, E. S. Evaluating Lipid Mediator Structural Complexity Using Ion Mobility Spectrometry Combined with Mass Spectrometry. *Bioanalysis* **2018**, *10* (5), 279–289. https://doi.org/10.4155/bio-2017-0245.

(3) Stow, S. M.; Causon, T. J.; Zheng, X.; Kurulugama, R. T.; Mairinger, T.; May, J. C.; Rennie, E. E.; Baker, E. S.; Smith, R. D.; McLean, J. A.; et al. An Interlaboratory Evaluation of Drift Tube Ion Mobility–Mass Spectrometry Collision Cross Section Measurements. *Anal. Chem.* **2017**, *89* (17), 9048–9055. https://doi.org/10.1021/acs.analchem.7b01729.